Journal of Solid Mechanics Vol. 12, No. 4 (2020) pp. 729-743

Vibration Analysis of the Sandwich Beam with Electro-Rheological Fluid Core Embedded Within Two FG Nanocomposite Faces Resting on Pasternak Foundation

A.H. Ghorbanpour-Arani *, A. Rastgoo

School of Mechanical Engineering, College of Engineering, University of Tehran, Tehran, Iran

Received 30 June 2020; accepted 31 August 2020

ABSTRACT

This investigation deals with the vibration analysis of the sandwich beam with electro-rheological (ER) core embedded within two functionally graded (FG) carbon nanotubes (CNTs) reinforced composite (FG-CNTRC) layers. In this regard, the governing equations are extracted by the Hamilton principle and the rule of mixture is employed to calculate the effective mechanical and physical properties of the CNTRCs face-sheets. Don and Yalcintas shear modulus models are applied to simulate shear modules of the ER core of the beam. The elastic medium is simulated by Winkler-Pasternak model and then, the governing equations are analytically solved. Finally, a parametric study is carried out in details and the effects of some main designing parameters such as applied voltage, Winkler coefficient, Pasternak coefficient, core to face-sheets thickness ratios and the different pattern of the CNTs along the face-sheets and loss factors are examined on the natural frequency. Based on the obtained results, volume fraction of CNTs in face-sheets have significant influence on the natural frequency in which by increasing the volume fractions the flexural rigidity of the sandwich beam increases as well as natural frequency.

Keywords: Electro-rheological core; Carbon nanotube; Composite material; Functionally graded layers.

1 INTRODUCTION

THE electro-rheological (ER) fluids are intelligent materials in which the elastic properties are varied by the applied electrical filed. As the most important features of ER fluids can be pointed to quick response, good reversibility and controllable performance which make them proper for use in various devices and structures. Such unique characteristics along with the inherent ability of electro-rheological fluids to interface with modern control systems make them very useful in numerous vibration and noise control applications such as shock absorbers, vibration damping devices, brakes, clutches, actuators, sensors, servo-valves, robotic joints, muscle stimulators and etc. (Lu and Li [17], Sun and Thomas [28], Krivenkov et al.[16], Norrick [19]). The use of an ER fluid for the

*Corresponding author.
E-mail address: *ahg.arani@gmail.com* (A.H. Ghorbanpour-Arani).

construction of smart structure components has been previously studied (Coulter [10], Weiss et.al. [34]). In other hand, the sandwich beams because of comprising three layers, middle layer co-called core embedded within two layers co-called face-sheets, have a high stiffness and therefore are appropriate to use in civil and mechanical structures (Cunedioglu [11], Poortabib and Naghsoudi [21], Ying et.al. [38]). Sandwich beams are utilized in a variety of engineering applications including aircraft, construction, and transportation where strong, stiff, and light structures are required (Bessaim [6]). In sandwich panels with non-metallic core, the core is more flexible than face sheets. In such structures, the softness of the core in the vertical direction is associated with localized effects in the form of localized displacements and stresses, which affect the safety of the overall panel (Biglari and Jafari [8]). CNTs have specified mechanical, physical and electronic properties that can be used for the reinforcement of polymer composites (Chemi et. al [9], Esawi and Farage [13], Rakrak et.al [23], Tounsi et.al [32]).Combination of nanotubes and CNTs leads to excellent properties for various applications. For example, the axial Young's modulus (Y_{axis}) of single-walled carbon nanotube (SWCNT) arrays with diameters of several micrometers is close to that of commercial high performance carbon fibers (CFs), but the specific Young's modulus (Y^{s}_{axis}) of SWCNT arrays is much better than that of high performance CFs (Besseghier et. al [7], Sun et.al.[27]). Chen et al. [36] studied the dynamic stability problem of a sandwich beam with a constrained layer and an ER fluid core subjected to an axial dynamic force. According to the obtained results in aforementioned investigation, the ER cores have a significant effect on the dynamic stability regions. The dynamic modeling and vibration characteristics of a rotating sandwich beam filled with an ER materials layer were investigated by Wei et al. [33]. They described the stress–strain relationship for the ER fluids by a complex shear modulus using linear visco-elasticity theory and concluded that significant vibration attenuation was achieved as the electric field was increased at different rotating speeds, and demonstrate the feasibility of using the ER fluids to control the vibration of the rotating beam. Ramkumar and Ganesan [24] presented vibration and damping analysis of composite sandwich box column containing ER core with constraining layer. They determined the modal loss factor and frequency of laminated composite box columns with integral viscoelastic/ER fluid layers using finite element based modal strain energy method. Allahverdizadeh et al.[2] scrutinized the vibration properties of a rotating Functionally Graded Electro-Rheological (FGER) beam. In mentioned research beam structure was comprised an ER fluid layer embedded between two functionally graded material layers. The results quantified the significant effect of the FGM distribution and the ER core on the vibration suppression of the rotating composite beam. In addition the vibration analysis of adaptive Timoshenko sandwich beams with ER fluid (ERF) core is examined by Allahverdizadeh et al [3]. Researchers evaluated the effects of thickness of the layers and applied electric fields on natural frequencies and modal loss factors. Rezaeepazhand et al. [29] in their investigation focused on dynamic stability of smart sandwich beams resting on Winkler elastic foundation subjected to harmonic axial loads. In order to increase the dynamic buckling load and the stability region of the beam, they connected an electro-rheological layer as a core in their beam and finally achieved that by applying electric field to the electro-rheological core, dynamic critical load and consequently, dynamic stability of the beam increase efficiently. Allahverdizadeh et al. [4] evaluated the Dynamic behavior of adaptive sandwich beams, manufacturing middle layer with ER fluid and constraining layers by functionally graded materials (FGM). Due to in aforementioned study, they considered the shear modulus of the viscoelastic core as a complex value therefore they concluded that this value has significant role in dynamic behavior of the beam. In addition, a dependable procedure was proposed to estimate this characteristic to ensure the reliability of the FE model for predicting the dynamic behavior of FGER beams. Also Allahverdizadeh et al. [1] analyzed amplitude-dependent dynamic characteristics of FGER sandwich beams. In their investigation nonlinear characteristics of the ER fluid layer was introduced and modeled by an exponential function. They carried out a detailing parametric study and checked effects of the different boundary conditions, applied electric fields, FGM volume fraction indices and thickness ratios on nonlinear fundamental frequency and modal loss factor ratio. The supersonic flutter control of a three-layered sandwich curved panel of rectangular plan form with an adaptive ERF core layer was investigated by Hasheminejad et al. [15]. The aero-elastic response of the cylindrical panel excited by an impulsive central point load was calculated using the Runge–Kutta time integration scheme. Pawlus [20] investigated dynamic response of three-layered annular plate with ER core subjected to time-dependent forces. He studied this problem as analytically and numerically using the orthogonalization method and the finite difference method. Recently, Ghorbanpour Arani et al. [14] presented differential quadrature method for vibration analysis of electro-rheological sandwich plate with CNT reinforced nanocomposite facesheets subjected to electric field. They utilized the Eshelby-Mori-Tanaka approach to obtain the material properties of nanocomposite face-sheets.

With respect to the presented literature review in this paper and according to the authors' knowledge, no report has been found in the case of vibration analysis of the sandwich beam with ER core embedded within two FG-CNTs face sheets carried out. Therefore, at first, the governing motion equations of the sandwich beam with ER core

embedded within FG-CNTRC face-sheets are derived. The Hamilton principle, Don, and Yalcintas shear modules models are employed to extract the governing equations. The surrounding elastic medium is modeled as Pasternak foundation and then, the governing equations are analytically solved. Finally, a parametric study is accomplished in details and the effects of some main parameters in designing such as applied voltage, Winkler coefficient, Pasternak coefficient, the core to face-sheets thickness ratios and the difference pattern of the CNT in thickness of the face-sheets on the natural frequency and loss factors are evaluated.

2 THE GOVERNING EQUATIONS

Considering a sandwich beam comprising an ER fluid core embedded within two reinforcement face-sheets with CNTs which is demonstrated in Fig.1. The beam rested on the Pasternak foundation can be depicted as follows:

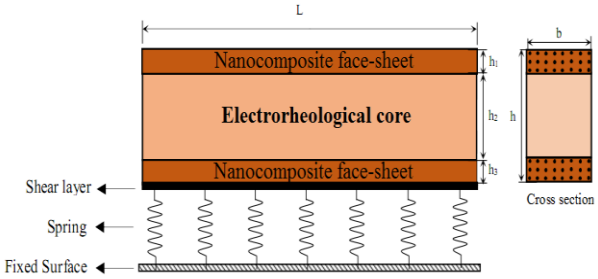

Fig.1
The sandwich beam geometrical with ER core and CNTRC face-sheets.

Before deriving of the motion equations, the following assumptions used in this work must be mentioned:

1. No slipping between the elastic and ER layers is assumed.
2. The transverse displacements for every point on a cross-section are the same.
3. There exists no normal stress in the ER layer, and there exists no shear strain in the elastic layer either.
4. The shear stress and strain properties of ER fluids are considered in the pre-yield regime.

2.1 The surrounding elastic medium is modeled as the Winkler-Pasternak model

In the same investigation, aforementioned assumptions were also used by (Wei et.al.[33], Yeh and Chen [37]). The effective properties of such reinforced composite can be computed by Mori–Tanaka scheme or by the rule of mixtures (Natarajan et. Al [18]). However, in this work the simple rule of mixture with correction factors is used to evaluate the effective material properties of CNTRC. The effective material properties of the CNTRC can be expressed by (Rafiee et.al. [22]):

$$\begin{aligned} E_{11sh} &= \eta_1 V_{cn} E_{11}^{CN} + V_m E^m \\ \alpha_{11sh} &= V_{cn} \alpha_{11}^{CN} + V_m \alpha^m \\ \tau_{11sh} &= V_{cn} \tau_d^{CN} + V_m \tau_d^m \\ \rho_{11sh} &= V_{cn} \rho^{CN} + V_m \rho^m \end{aligned} \tag{1}$$

In above equation, E_{11}^{CN}, α_{11}^{CN}, τ_{11}^{CN} and ρ_{11}^{CN} are the Young's module, the expansion coefficient, the viscoelastic coefficient and density, respectively of the CNTs and E^m, α^m, τ^m and ρ^m are the corresponding properties for the matrix. Furthermore, V_{cn} and V_m are the CNTs and matrix volume fractions and are related by (Shen and Zhang [26]). The FG distributions of the CNTs along the thickness direction of the face-sheets are given by:

$$V_{CN}^{t}=\frac{\left(2z-h_2\right)}{h_3}V_{CN}^{*}$$
$$V_{CN}^{b}=-\frac{\left(2z+h_2\right)}{h_1}V_{CN}^{*} \tag{2}$$

where V_{CN}^{t} and V_{CN}^{b} represent the volume fractions of the CNTs for top and bottom face-sheets, respectively, and V_{CN}^{*} can be calculated as follows:

$$V_{CN}^{*}=\frac{w_{CN}}{w_{CN}+\left(\frac{\rho^{CN}}{\rho^{m}}\right)-\left(\frac{\rho^{CN}}{\rho^{m}}\right)w_{CN}} \tag{3}$$

In which, w_{CN} is the mass fraction of the CNTs. It should be noted that V_{CN}^{t} and V_{CN}^{b} are equal to V_{CN}^{*} for uniform distribution (UD) of CNTs in face-sheets, while for FG distribution defined in Eq. (2), CNTs are linearly distributed from the inside to outside of face-sheets.

The Pasternak model to simulate of the elastic medium is presented as follow:

$$F_{elastic\ medium}=-K_w W+K_P\left(\frac{\partial^2 W}{\partial x^2}\right) \tag{4}$$

where K_w and K_P are the Winkler and Pasternak coefficients, respectively. Next, the displacement relation of the face-sheets can be expressed as (see Fig. 2):

$$\overline{u}_i\left(x,z,t\right)=u_i\left(x,t\right)-z_i\frac{\partial w_0\left(x,t\right)}{\partial x} \qquad i=1,3$$
$$w\left(x,t\right)=w_0\left(x,t\right) \tag{5}$$

In which, $\overline{u}_i$ is the axial displacement of the each face-sheets and *w* is the transverse displacement of the three layers. Furthermore, u_i is the axial displacement of the mid-plane of layer *i*, and z_i is the distance of the mid-height of layer *i*. Therefore, the strain- displacement using infinitesimal theory of elasticity and green strain tensor can be calculated as (Allahverdizadeh et.al. [2], Hasheminejad and Aghayi Motaaleghi [15]):

$$\varepsilon_{xxi}=\frac{\partial u_i\left(x,t\right)}{\partial x}-z_i\frac{\partial^2 w_0\left(x,t\right)}{\partial x^2} \qquad i=1,3 \tag{6}$$

In addition, with considering strain-displacement relation in ER core, the shear deformation can be expressed as:

$$\gamma_{xz\,2}=\frac{\partial w\left(x,t\right)}{\partial x}+\frac{\partial u_2\left(x,t\right)}{\partial z} \tag{7}$$

In which, u_2 is the axial displacement in the core of the beam. With attention to Fig. 2, it is possible that first term in Eq. (7) expresses as function of the axial displacement in two elastic layers as the form:

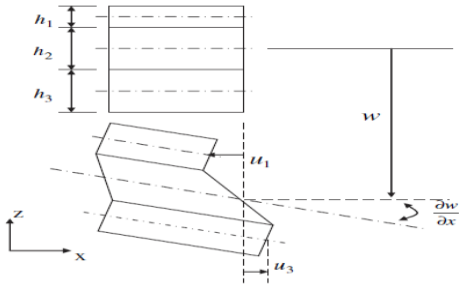

Fig.2
Un-deformed and deformed configurations of a sandwich beam (Rezaeepazhand and Pahlavan [25]).

$$\frac{\partial u_2(x,t)}{\partial z} = \frac{\Delta u_{rotation} + \Delta u_{elongation}}{h_2} = \frac{1}{h_2}\left(\frac{h_1}{2} + \frac{h_3}{2}\right)\frac{\partial w(x,t)}{\partial x} + \frac{u_1(x,t) - u_3(x,t)}{h_2}$$
$$= \frac{h_1 + h_3}{2h_2}\frac{\partial w(x,t)}{\partial x} + \frac{u_1(x,t) - u_3(x,t)}{h_2} \tag{8}$$

Then compatibility relation is written as (see Fig. 3):

$$\gamma_{xz\,2} = \frac{d}{h_2}\frac{\partial w(x,t)}{\partial x} + \frac{u_1(x,t) - u_3(x,t)}{h_2} \tag{9}$$

In which d is equal to $d = \frac{h_1}{2} + h_2 + \frac{h_3}{2}$,

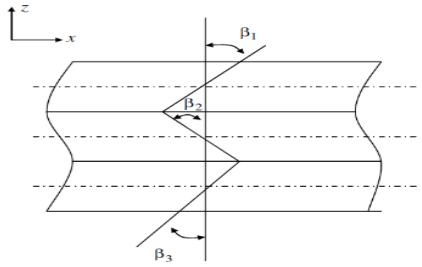

Fig.3
The compatibility relation in sandwich beam.

The Hamilton principle is used to drive the governing equations of motion. It is presented as:

$$\int_0^t \delta(K_{Sandwich} - (U_{Sandwich} + \Omega_{Elastic\ medium}))dt = 0 \tag{10}$$

where K, U and Ω are the kinetic energy, the strain energy and the work done by external force, respectively. Thus, the strain energy is written for each layer separately as the form:

$$U_{Sandwich} = U_{face\ sheets} + U_{ER\ core}$$

$$U_{Face\ sheets} = U^{Bottom}_{Face\ sheet} + U^{Top}_{Face\ sheet} = \frac{1}{2}\int_{-h_3-\frac{h_2}{2}}^{-\frac{h_2}{2}}\int_0^b\int_0^a \left(\sigma_{ij}\varepsilon_{ij} + \tau_{ij}\gamma_{ij}\right)_{Sheet} dx\,dy\,dz + \frac{1}{2}\int_{\frac{h_2}{2}}^{\frac{h_2}{2}+h_1}\int_0^b\int_0^a \left(\sigma_{ij}\varepsilon_{ij} + \tau_{ij}\gamma_{ij}\right)_{Sheet} dx\,dy\,dz. \tag{11}$$

$$U_{ER\ core} = \int_V G_2\left(\gamma^2_{xz\,2}\right)dV$$

In above equation, G_2 is the complex shear modulus of the ER core that expressed as a function of the electrical filed based on two models explained as:

$$G_2^D = G' + iG'' \rightarrow \begin{cases} G' \approx 15000E^2 \\ G'' \approx 6900 \end{cases}$$
$$G_2^Y = G' + iG'' \rightarrow \begin{cases} G' \approx 50000E^2 \\ G'' \approx 2600E + 1700 \end{cases}, \tag{12}$$

where G_2^D and G_2^Y are the complex shear modulus based on Don and Yalcintas models, respectively (Don [12], Yalcintas and Coulter [35]). Also in Eq. (12), E is applied electrical filed. Furthermore, the kinetic energy of the sandwich beam has the following three parts (Allahverdizadeh et.al. [2], Yeh and Chen [37]):

$$K_{Face\ sheets} = \frac{1}{2}\int_A [\rho_1 h_1 \left(\frac{\partial u_1(x,t)}{\partial t}\right)^2 + \rho_3 h_3 \left(\frac{\partial u_3(x,t)}{\partial t}\right)^2] dx\ dy$$
$$K_{Face\ sheets\ \&\ ER\ core} = \frac{1}{2}\int_A \left(\rho_1 h_1 + h_2\rho_2 + \rho_3 h_3\right)\left(\frac{\partial w_0(x,t)}{\partial t}\right)^2 dx\ dy \tag{13}$$
$$K_{ER\ core} = \frac{1}{2}\int_A I_2 \dot{\gamma}_{xz\,2}^2\ dx\ dy$$

In above equation, $K_{Face\ sheets}$, $K_{Face\ sheets\ \&\ ER\ core}$ and $K_{ER\ core}$ are the axial kinetic energy for both face-sheets, the transvers kinetic for three layers and the kinetic energy resulted shear strain in ER core, respectively. In addition, other parameters in Eq. (13) are calculated as:

$$(\rho_1, \rho_3) = \int_{h_1 or\ h_2} \rho(z_i) dz_i, \qquad i = 1, 3$$
$$I_2 = \rho_2 \frac{h_2^3}{12} \tag{14}$$

The work done by force resulted Winkler-Pasternak foundation is expressed as follows:

$$\Omega_{Elastic\ medium} = \frac{1}{2}\int_0^L F_{Elastic\ medium}\ w\ dx \tag{15}$$

Finally, substituting Eqs. (11), (13), and (15) into Eq. (10), in conjunction with other equations, the dynamic equations of the top face-sheet are obtained as:

$$\delta U_1 = 0: \quad 2G\alpha_2 \frac{\partial}{\partial\eta} W(\eta,\tau) + 2\frac{GU_1(\eta,\tau)}{\alpha_2} + G\alpha_1 \frac{\partial}{\partial\eta} W(\eta,\tau) + 1/24\alpha_1 \frac{\partial^3}{\partial\tau^2\partial\eta} W(\eta,\tau) + 1/24\alpha_3 \frac{\partial^3}{\partial\tau^2\partial\eta} W(\eta,\tau)$$
$$-2\frac{GU_3(\eta,\tau)}{\alpha_2} + G\alpha_3 \frac{\partial}{\partial\eta} W(\eta,\tau) + \frac{\varrho\delta\frac{\partial^2}{\partial\tau^2} U_1(\eta,\tau)}{\alpha_2} - \alpha_1 \frac{\partial^2}{\partial\eta^2} U_1(\eta,\tau) + 1/12\alpha_2 \frac{\partial^3}{\partial\tau^2\partial\eta} W(\eta,\tau) \tag{16}$$
$$+1/12\frac{\frac{\partial^2}{\partial\tau^2} U_1(\eta,\tau)}{\alpha_2} - 1/12\frac{\frac{\partial^2}{\partial\tau^2} U_3(\eta,\tau)}{\alpha_2} = 0$$

and also the equation of motion for bottom face-sheet is calculated as the following form:

$$\delta U_3 = 0: \quad -G\alpha_1 \frac{\partial}{\partial \eta} W(\eta,\tau) - 2G\alpha_2 \frac{\partial}{\partial \eta} W(\eta,\tau) - G\alpha_3 \frac{\partial}{\partial \eta} W(\eta,\tau) - 1/24\alpha_1 \frac{\partial^3}{\partial \tau^2 \partial \eta} W(\eta,\tau) - 1/12\alpha_2 \frac{\partial^3}{\partial \tau^2 \partial \eta} W(\eta,\tau)$$
$$-1/24\alpha_3 \frac{\partial^3}{\partial \tau^2 \partial \eta} W(\eta,\tau) + \frac{\left(\frac{\partial^2}{\partial \tau^2} U_3(\eta,\tau)\right)\epsilon\varrho}{\alpha_2} - \left(\frac{\partial^2}{\partial \eta^2} U_3(\eta,\tau)\right)\alpha_3 + 2\frac{GU_3(\eta,\tau)}{\alpha_2} - 2\frac{GU_1(\eta,\tau)}{\alpha_2} \tag{17}$$
$$+1/12\frac{\frac{\partial^2}{\partial \tau^2} U_3(\eta,\tau)}{\alpha_2} - 1/12\frac{\frac{\partial^2}{\partial \tau^2} U_1(\eta,\tau)}{\alpha_2} = 0$$

Eventually, governing equation for core layer is evaluated as:

$$\delta W = 0: \quad -2\left(\frac{\partial}{\partial \eta} U_1(\eta,\tau)\right)G + 2\left(\frac{\partial}{\partial \eta} U_3(\eta,\tau)\right)G - \left(\frac{\partial}{\partial \eta} U_1(\eta,\tau)\right)G\varepsilon + \left(\frac{\partial}{\partial \eta} U_3(\eta,\tau)\right)G\varepsilon - 1/12\alpha_1\left(\frac{\partial^4}{\partial \tau^2 \partial \eta^2} W(\eta,\tau)\right)\alpha_2$$
$$+\left(\frac{\partial^2}{\partial \tau^2} W(\eta,\tau)\right)\epsilon\varrho - 1/2\left(\frac{\partial^2}{\partial \eta^2} W(\eta,\tau)\right)\alpha_1^2 G - 2\left(\frac{\partial^2}{\partial \eta^2} W(\eta,\tau)\right)\alpha_2^2 G - 1/2\left(\frac{\partial^2}{\partial \eta^2} W(\eta,\tau)\right)\alpha_3^2 G + \left(\frac{\partial^2}{\partial \tau^2} W(\eta,\tau)\right)\varrho\delta$$
$$-1/24\alpha_1\left(\frac{\partial^4}{\partial \tau^2 \partial \eta^2} W(\eta,\tau)\right)\alpha_3 - 1/12\left(\frac{\partial^4}{\partial \tau^2 \partial \eta^2} W(\eta,\tau)\right)\alpha_2\alpha_3 + \alpha_1^3\alpha_2 I_1 \frac{\partial^4}{\partial \eta^4} W(\eta,\tau) + \alpha_3^3\alpha_2 I_3 \frac{\partial^4}{\partial \eta^4} W(\eta,\tau)$$
$$-2\alpha_1\left(\frac{\partial^2}{\partial \eta^2} W(\eta,\tau)\right)\alpha_2 G - \alpha_1\left(\frac{\partial^2}{\partial \eta^2} w(\eta,\tau)\right)\alpha_3 G - 2\left(\frac{\partial^2}{\partial \eta^2} W(\eta,\tau)\right)\alpha_2\alpha_3 G - I_1\left(\frac{\partial^4}{\partial \tau^2 \partial \eta^2} W(\eta,\tau)\right)\alpha_1^2\varrho\delta$$
$$-I_3\left(\frac{\partial^4}{\partial \tau^2 \partial \eta^2} W(\eta,\tau)\right)\alpha_3^2\epsilon\varrho - 1/12\frac{\partial^3}{\partial \tau^2 \partial \eta} U_1(\eta,\tau) + 1/12\frac{\partial^3}{\partial \tau^2 \partial \eta} U_3(\eta,\tau) + \frac{\partial^2}{\partial \tau^2} W(\eta,\tau) - 1/48\left(\frac{\partial^4}{\partial \tau^2 \partial \eta^2} W(\eta,\tau)\right)\alpha_3^2 \tag{18}$$
$$-1/24\left(\frac{\partial^3}{\partial \tau^2 \partial \eta} U_1(\eta,\tau)\right)\delta + 1/24\left(\frac{\partial^3}{\partial \tau^2 \partial \eta} U_3(\eta,\tau)\right)\delta - 1/24\left(\frac{\partial^3}{\partial \tau^2 \partial \eta} U_1(\eta,\tau)\right)\epsilon$$
$$1/24\left(\frac{\partial^3}{\partial \tau^2 \partial \eta} U_3(\eta,\tau)\right)\epsilon - 1/48\left(\frac{\partial^4}{\partial \tau^2 \partial \eta^2} W(\eta,\tau)\right)\alpha_1^2 - 1/12\left(\frac{\partial^4}{\partial \tau^2 \partial \eta^2} W(\eta,\tau)\right)\alpha_2^2$$
$$-\left(\frac{\partial}{\partial \eta} U_1(\eta,\tau)\right)G\delta + \left(\frac{\partial}{\partial \eta} U_3(\eta,\tau)\right)G\delta - K_w w_0(x,t) + K_p \frac{\partial^2}{\partial x^2} w_0(x,t) = 0$$

It is noted that the governing equation with using the following new variables are dimensionless.

$$K_w = \frac{h_2}{\bar{C}_{11}} k_w, \; K_p = \frac{k_p}{L.\bar{C}_{11}}, \quad \eta = \frac{x}{L}, \quad (U_i, W) = \left(\frac{u_i}{L}, \frac{w}{h_2}\right) \qquad i = (1,3),$$
$$\alpha_i = \frac{h_i}{L} \qquad i = (1,2,3), \quad G = \frac{G_2}{\bar{C}_{11}}, \quad \epsilon = \frac{h_3}{h_2}, \quad \delta = \frac{h_1}{h_2}, \quad \varrho = \frac{\rho_{1or3}}{\rho_2}, \quad \tau = \frac{t}{h_2}\sqrt{\frac{\bar{C}_{11}}{\rho_2}}, \quad I_1 = I_3 = \frac{1}{12}. \tag{19}$$

3 SOLUTION METHOD

In this section, the Navier's solution is employed to solve the governing motion equations of the sandwich beam with ER core embedded two reinforcement CNTs face-sheets obtained in previous sections (Thai et.al [31]). Regarding to solution procedure, displacement functions are considered as the following form:

$$U_1(\eta,\tau)=\sum_{m=1}^{\infty}U_{1m}\cos(m\pi\eta)e^{i\varpi\tau}$$
$$U_3(\eta,\tau)=\sum_{m=1}^{\infty}U_{3m}\cos(m\pi\eta)e^{i\varpi\tau} \quad (20)$$
$$W(\eta,\tau)=\sum_{m=1}^{\infty}W_m\sin(m\pi\eta)e^{i\varpi\tau}$$

In Eq. (20), m demonstrates the number of mode shapes and $\bar{\omega}$ is the dimensionless natural frequency that using $\omega=\bar{\omega}\times\left(\frac{1}{h_2}\sqrt{\frac{\bar{c}_{11}}{\rho_2}}\right)$ is dimension. Then, substituting Eq. (20) in Eqs. (16-18), the eigenvalues problem form is obtained as:

$$\left\{\begin{bmatrix}k_{11}&k_{12}&k_{13}\\k_{21}&k_{22}&k_{23}\\k_{31}&k_{32}&k_{33}\end{bmatrix}-\omega_n^2\begin{bmatrix}m_{11}&m_{12}&m_{13}\\m_{21}&m_{22}&m_{23}\\m_{31}&m_{32}&m_{33}\end{bmatrix}\right\}\begin{Bmatrix}u_1\\u_3\\w\end{Bmatrix}=0 \quad (21)$$

where coefficient in above equation is calculated and presented in Appendix A. Finally, with solving the mentioned eigenvalues problem, the natural frequency is obtained as the complex form that dividing the imaginary part to real part of the natural frequency results loss factor (Allahverdizadeh et.al. [2], Allahverdizadeh et.al. [3]).

4 RESULTS AND DISCUSSION

The material properties and geometrical features of the sandwich beam with ER core embedded within two CNTs reinforcement face-sheets are presented in Table 1 (Yeh and Chen [36]).

Table 1
The material and geometrical properties of the constituent material of the beam (Yeh and Chen [36]).

Geometrical parameters	$h_1=0.5\ mm, h_2=2\ mm, h_3=0.5\ mm, L=300\ mm$
The mechanical properties of top and bottom face sheets	$\rho_1=\rho_3=1150\ kg/m^3,\ \nu_1=\nu_3=0.34$ $E_1=E_3=(3.52-0.0034T)\ Gpa, (T=T_0+\Delta T, T_0=300K)$ $E_1(300K)=E_3(300K)=2.5\ Gpa$

To justify the accuracy of the present issue for solution of different problems, the obtained results are compared with existing results of literature. According to Ref. (Allahverdizadeh et.al. [4], Arikoglu and Ozkol [5], Tang and Lumsdaine [30]) the property and characteristics of the beam consider as follows:

Table 2
The material and geometrical properties of the constituent material of the beam according to Ref. (Allahverdizadeh et.al. [4], Arikoglu and Ozkol [5], Tang and Lumsdaine [30]).

Geometrical parameters	$h_1=5\ mm, h_2=2.5\ mm, h_3=0.5\ mm, L=300\ mm$
The mechanical properties of top and bottom face sheets	$\rho_1=\rho_3=7800\ kg/m^3, \rho_2=2000\ kg/m^3,$ $E_1=E_3=207\ Gpa, G_2=0.2615(1+0.38i)\ MPa$

with respect to the obtained results in this work and results from three others references presented in Table 3, it can be seen that maximum difference between frequencies in fundamental mode is approximately % 0.589 and for frequency in higher mode is % 0.2. These difference is acceptable measurements and explains high precise in solution procedure and justify the extracting motion equations.

Table 3
Comparison between obtained frequency in this work and Ref. (Allahverdizadeh et.al. [4], Arikoglu and Ozkol [5], Tang and Lumsdaine [30]).

	Mode 4	Mode 3	Mode 2	Mode 1
Present work	11767.09	6627.80	2952.192	744.815
Ref.(Allavrdizadeh , Mahjoob, Maleki, et.al. [4])	11717.3	6608.93	2944.89	740.306
Ref.(Arikoglu and Ozkol [5])	11763.52	6623.477	2947.775	740.489
Ref.(Tang and Lumsdaine [30])	11782.61	6629.68	2949.00	740.564

In addition, the comparison presented in Table 4 between the obtained loss factor in present work and Refs. (Allahverdizadeh et.al. [4], Arikoglu and Ozkol [5], Tang and Lumsdaine [30]) indicate that the current method has capability to evaluate the responses with acceptable accuracy. As can be seen in this table, the maximum difference is approximately % 3.1202 for fundamental mode and is smaller than % 1.00 for other higher mode shapes.

Table 4
Comparison between obtained loss factors in this work and Ref. (Allahverdizadeh et.al. [4], Arikoglu and Ozkol [5], Tang and Lumsdaine [30]).

	Mode 4	Mode 3	Mode 2	Mode 1
Present work	0.028831	0.05107897	0.113877	0.434226
Ref. (Allavrdizadeh, Mahjoob, Maleki et.al. [4])	0.0288852	0.0512581	0.114795	0.448204
Ref. (Arikoglu and Ozkol [5])	0.028859	0.051232	0.11477	0.44818
Ref. (Tang and Lumsdaine [30])	0.028932	0.051306	0.11484	0.44825

In Fig. 4, based on the geometrical and material property listed in Table 5, another comparison is accomplished between results obtained by the Navier's solution and finite element presented in Ref. (Yeh et.al. [37]).

Table 5
The material and geometrical properties of the constituent material of the beam according to Ref. (Yeh et.al. [37]).

Geometrical parameters	$h_1 = 0.079\ mm, h_2 = 0.79\ mm, h_3 = 0.79\ mm, L = 381\ mm$
The mechanical properties of top and bottom face sheets	$\rho_1 = \rho_3 = 2700\ kg/m^3, \rho_2 = 1200\ kg/m^3,$ $E_1 = E_3 = 70Gpa, G_2 = (50000E*^2 + (2600E* + 1700)i)\ Pa$

Based on the Fig. 4, the Navier solution has acceptable results with other outputs which were represented in literatures.

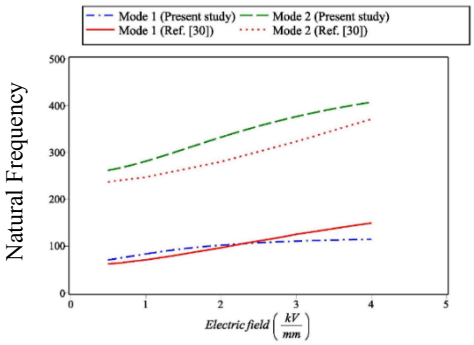

Fig.4
The evaluation obtained results by comparison with results presented in Ref. (Yeh et.al [36]).

Fig. 5 illustrates the natural frequency in terms of applied electrical field (E) for simply supported and two difference ER models. According to this figure, the natural frequency increases with increasing applied electrical field E. It can be concluded that the flexural stiffness of sandwich beam is increased with increasing aforementioned parameter (E). ER fluids can be changed from liquid to quasi-solid phase subjected to the external electric field. In order to change the phase from liquid to solid, particles with electrical properties join together rapidly by applying the external electric field and form chain like and columnar structures in the electric field direction. Indeed, increasing electrical filed caused that shearing module of ER enhances therefore with attention to equations of motion; this varying appears in the increasing of natural frequency. Also, in larger applied electrical field, the

difference between two models (Don [12],Yalcintas [35]) is significant and cannot disregard from it as increasing the electrical field causes the elasticity modules for Yalcintas model.

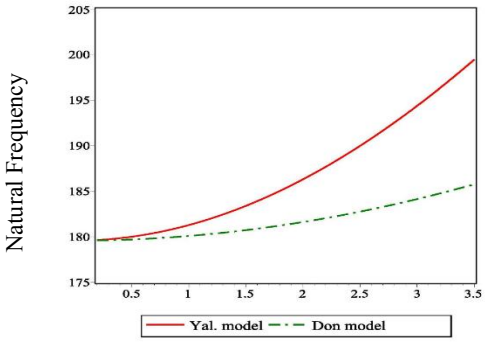

Fig.5
The natural frequency versus applied electrical field for two ER model.

In Fig. 6 the influences of the Pasternak coefficient (K_p) and Winkler coefficient (K_w) on the natural frequency is investigated. It can be concluded that increase in the both aforementioned coefficients lead to enhance the natural frequency magnitudes. Thus, by using Winkler-Pasternak foundation, the natural frequency increases and this enlargement becomes more prominent when the shear layer constant increases.

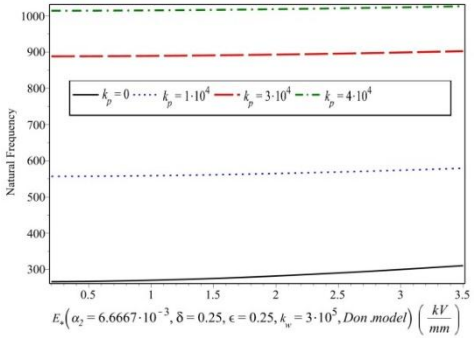

(a) Don model

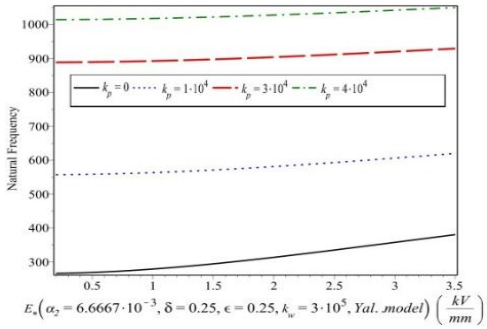

(b)Yalcintas model

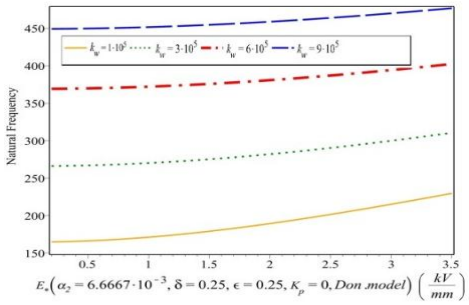

(c) Don model

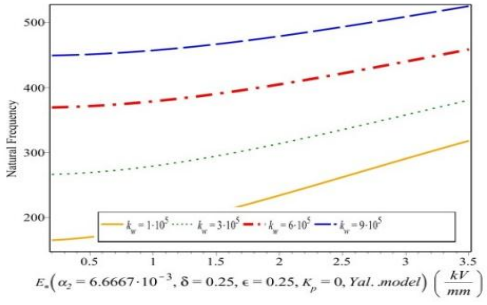

(d)Yalcintas model

Fig.6
The natural frequency versus applied electrical field for various K_p and K_w.

The effects of thickness of core to length of beam α_2 are presented in Fig. 7. As can be seen in this figure, increasing aforementioned ratio leads to enhance natural frequency for both elasticity models. The results of Fig. 7 indicate that the increasing α_2 values makes the flexural rigidity enhances and therefore, it causes to increase the natural frequency amounts.

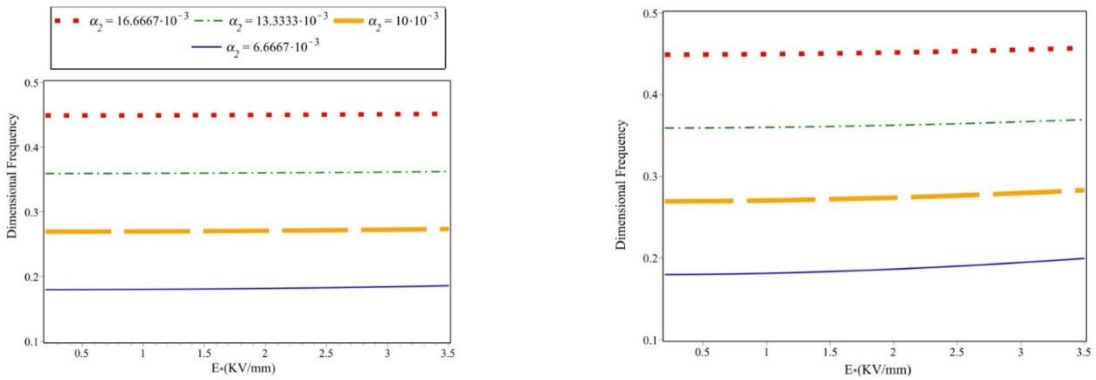

(a) Don model (b) Yalcintas model

Fig.7
The natural frequency versus applied electrical field for various α_2 .

The natural frequency versus electric field is represented in Fig. 8 for various face-sheets to core thickness ratios δ . It is clear that based on this figure, in both model, increasing aforementioned parameter causes increasing the natural frequency. It's due to the ER core is very softer than nanocomposite facesheets. Indeed, increasing of the thickness ratio have a more effects on the mass matrix respect to stiffness matrix as this incident caused that mass matrix increases.

The loss factor is presented in terms of applied electrical filed which is plotted in Fig. 9. Regarding to this figure can be deduced that increasing electrical field has different effect on loss factor for both Don and Yancintas models. Enhancing electrical field causes loss factor increases for Yancintas model and leads to decrease loss factor for Don Model. Based on Eq. (12), the imaginary part of complex shear modulus of ER core is constant for Don model and just increasing electrical field leads to increase real part of complex shear modulus and consequently, loss factor decreases. However, for Yancintas model, both the imaginary and real parts of complex shear modulus are variable relative to the electrical field and according to the Fig. 9(b), increasing electrical field causes to increase the dissipated energy in the system.

In Fig. 10, the natural frequency magnitudes are presented in terms of applied electrical field for various volume fractions of CNTs in face-sheets. It can be concluded that volume fraction of CNTs in face-sheets have significant influence on natural frequency as by increasing the volume fractions makes flexural rigidity of the sandwich beam increases as well as natural frequency.

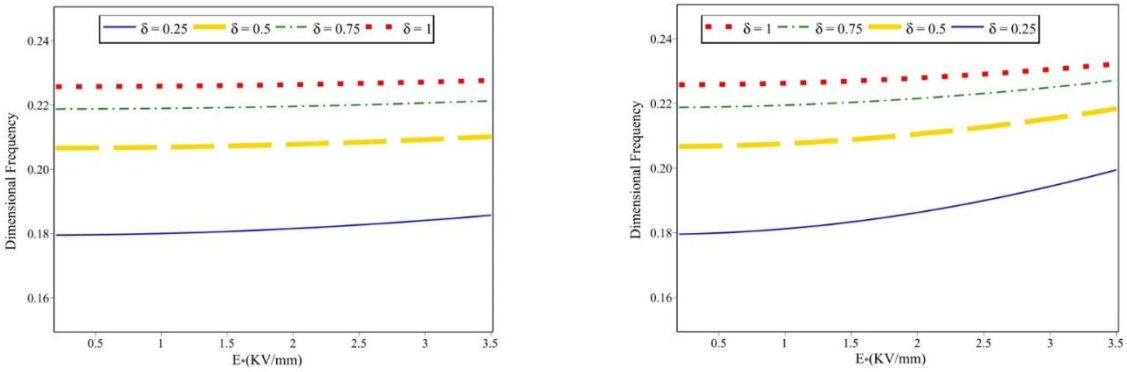

(a) Don model (b) Yalcintas model

Fig.8
The natural frequency versus applied electrical field for various δ .

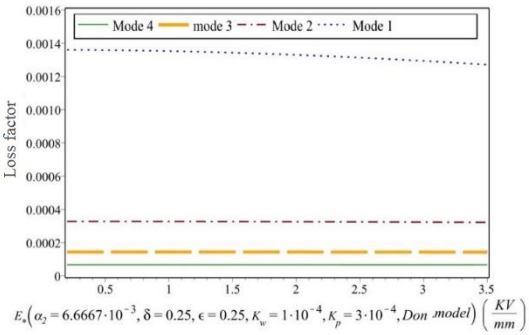

(a) Don model

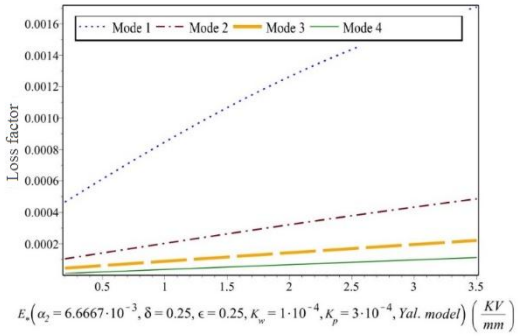

(b) Yalcintas model

Fig.9
The loss factor versus applied electrical field for various modes.

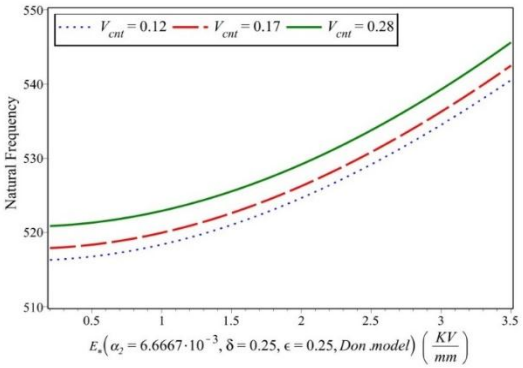

(a) Don model

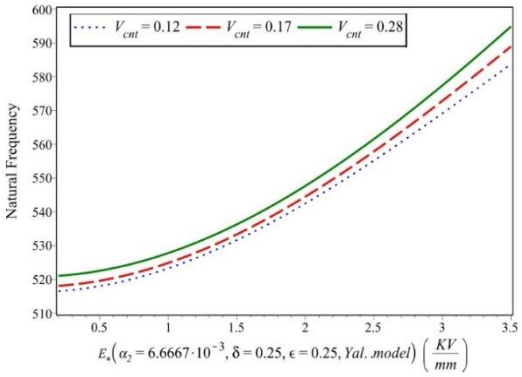

(b) Yalcintas model

Fig.10
The natural frequency versus applied electrical field for various volume fractions V_{CNT}.

The natural frequency versus applied electrical field for UD and FG distributions of CNT is demonstrated in Fig. 11. It can be found that FG distribution gives higher natural frequencies rather than UD distribution. Generally, the employing FG distribution of CNT is an effective manner to achieve greater stiffness. According to the obtained results in this figure and based on Eq. (2) for a same volume fraction, instead of uniformly distribution of CNTs in the matrix, if the accumulation of CNTs increases at the outer edges of face-sheets compared with the inner edges, the greater stiffness will be achieve for sandwich structure.

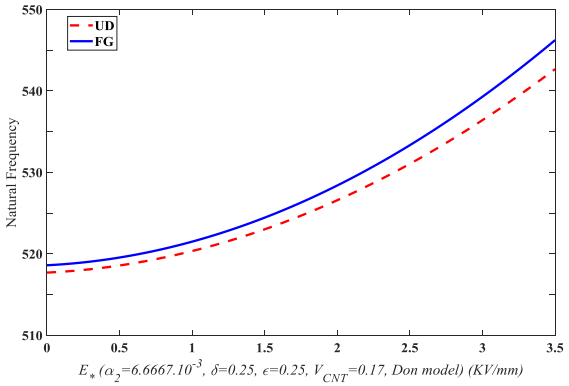

(a) Don model

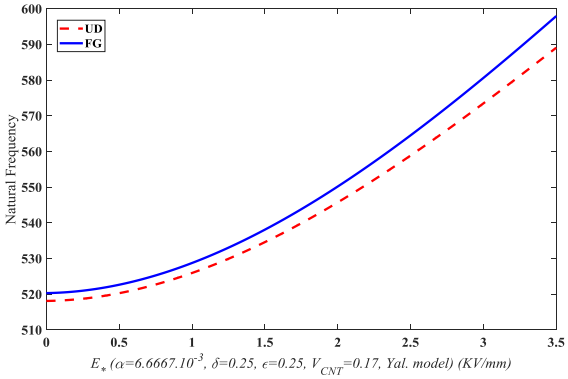

(b) Yalcintas model

Fig.11
The natural frequency versus applied electrical field for UD and FG distributions of CNT.

5 CONCLUSIONS

This study investigated the vibration analysis of the sandwich beam with ER core embedded within two FG-CNTRCs rested on Winkler-Pasternak foundation for the first time. In this regard, the governing equation is extract by the Hamilton principle and the rule of mixture is employed in order to calculate the effective mechanical and physical properties of the CNTRCs face-sheets. Don and Yalcintas shear modules models are applied to simulate shear modules of the ER core of the beam. After solving analytically the equation of motion and calculated the natural frequency values, a parametric study accomplished in detail in which the following conclusions can be expressed:

1. The value of natural frequency of the sandwich beam depends on the model used for complex shear modulus of ER core. In the absence of the electric field, the variations of natural frequency are same for two model while the natural frequency calculated by Yancintas model is more than Don Model in the presence of the electric field.
2. It can be concluded that volume fraction of CNTs in face-sheets have significant influence on natural frequency as by increasing the volume fractions makes flexural rigidity of the sandwich beam increases as well as natural frequency.
3. Increasing electrical field values has different effect on loss factor for both Don and Yancintas models. Enhancing electrical field magnitudes causes loss factor increases for Yancintas model and leads to decrease loss factor for Don Model.
4. Increasing the face-sheets to core thickness ratio and thickness of the core to length of the beam ratio leads to increment of the natural frequency for both shear elasticity models.

APPENDIX A

$$m_{11}=\frac{\varrho\delta}{\alpha_2}+\frac{1}{12\alpha_2},\qquad m_{12}=-\frac{1}{12\alpha_2},\qquad m_{13}=1/\,24\alpha_1 m\pi+1/\,24\alpha_3 m\pi+1/\,12\alpha_2 m\pi,$$

$$m_{21}=-\frac{1}{12\alpha_2},\qquad m_{22}=\frac{\epsilon\varrho}{\alpha_2}+\frac{1}{12\alpha_2},\qquad m_{23}=-1/\,24\alpha_1 m\pi-1/\,12\alpha_2 m\pi-1/\,24\alpha_3 m\pi,$$

$$m_{31}=1/\,24\delta m\pi+1/\,24\epsilon m\pi+1/\,12m\pi,\qquad m_{32}=-1/\,24\delta m\pi-1/\,24\epsilon m\pi-1/\,12m\pi,$$

$$m_{33}=1+1/\,12\alpha_2\alpha_3 m^2\pi^2+1/\,12\alpha_1\alpha_2 m^2\pi^2+1/\,48\alpha_3{}^2 m^2\pi^2+1/\,48\alpha_1{}^2 m^2\pi^2$$
$$+1/\,12\alpha_2{}^2 m^2\pi^2+\epsilon\varrho+\varrho\delta+1/\,24\alpha_1\alpha_3 m^2\pi^2+I_3\alpha_3{}^2\epsilon\varrho m^2\pi^2+I_1\alpha_1{}^2\varrho\delta m^2\pi^2$$

$$k_{11}=2\frac{G}{\alpha_2}+\alpha_1 m^2\pi^2,\qquad k_{12}=-2\frac{G}{\alpha_2},\qquad k_{13}=G\pi m\alpha_1+2G\pi m\alpha_2+G\pi m\alpha_3,$$

$$k_{21}=-2\frac{G}{\alpha_2},\qquad k_{22}=\alpha_3 m^2\pi^2+2\frac{G}{\alpha_2},\qquad k_{23}=-\pi m\alpha_1 G-2\pi m\alpha_2 G-\pi m\alpha_3 G,$$

$$k_{31}=2G\pi m+\pi\delta mG+\pi m\epsilon G,\qquad k_{32}=-\pi\delta mG-\pi m\epsilon G-2\pi mG,$$

$$k_{33}=-\pi\delta mG-\pi m\epsilon G-2\pi mG.$$

REFERENCES

[1] Allahverdizadeh A., Eshraghi I., Mahjoob M.J., Nasrollahzadeh N., 2014, Nonlinear vibration analysis of FGER sandwich beams, *International Journal of Mechanical Sciences* **78**: 167-176.

[2] Allahverdizadeh A., Eshraghi I., Asgharifard S.P., 2012, Effects of electrorheological fluid core and functionally graded layers on the vibration behavior of a rotating composite beam, *Meccanica* **47**: 1945-1960.

[3] Allahverdizadeh A., Mahjoob M.J., Eshraghi I., Nasrollahzadeh N., 2013, On the vibration behavior of functionally graded electrorheological sandwich beams, *International Journal of Mechanical Sciences* **70**: 130-139.

[4] Allahverdizadeh A., Mahjoob M.J., Maleki M., Nasrollahzadeh N., Naei M.H., 2013, Structural modeling, vibration analysis and optimal viscoelastic layer characterization of adaptive sandwich beams with electrorheological fluid core, *Mechanics Research Communications* **51**: 15-22.

[5] Arikoglu A., Ozkol I., 2010, Vibration analysis of composite sandwich beams with viscoelastic core by using differential transform method, *Composite Structures* **416**(12): 3031-3039.

[6] Bessaim A., Houari M.S., Tounsi A., Mahmoud S., Abbes Adda Bedia E., 2013, A new higher-order shear and normal deformation theory for the static and free vibration analysis of sandwich plates with functionally graded isotropic face sheets, *Journal of Sandwich Structures and Materials* **15**(6): 671-703.

[7] Besseghier A., Heireche H., Anis Bousahla A., Tounsi A., Benzair A., 2015, Nonlinear vibration properties of a zigzag single-walled carbon nanotube embedded in a polymer matrix, *Advances in Nano Research* **3**(1): 29-37.

[8] Biglari H., Jafari A.A., 2010, Static and free vibration analyses of doubly curved composite sandwich panels with soft core based on a new three-layered mixed theory, *Proceedings of the Institution of Mechanical Engineers, Part C: Journal of Mechanical Engineering Science* **224**(11): 2332-2349.

[9] Chemi A., Heireche H., Zidour M., Rakrak K., Anis Bousahla A., 2015, Critical buckling load of chiral double-walled carbon nanotube using non-local theory elasticity, *Advances in Nano Research* **3**(4): 193-206.

[10] Coulter J. P., 1993, Engineering application of electrorheological materials, *Journal of Intelligent Material Systems and Structures* **4**: 248-259.

[11] Cunedioglu Y., 2015, Free vibration analysis of edge cracked symmetric functionally graded sandwich beams, *Structural Engineering and Mechanics* **56**(6): 4590-4597.

[12] Don D.L., 1993, *An Investigation of Electrorheologial Material Adaptive Structures*, Theses and Dissertations, Mechanical Engineering and Mechanics, Lehigh University.

[13] Esawi A., Farag M., 2007, Carbon nanotube reinforced composites: potential and current challenges, *Material & Design* **28**: 2394-2401.

[14] Ghorbanpour Arani A., Jamali S.A., BabaAkbar Zarei H., 2017, Differential quadrature method for vibration analysis of electro-rheological sandwich plate with CNT reinforced nanocomposite facesheets subjected to electric field, *Composite Structures* **180**: 211-220.

[15] Hasheminejad S.M., Aghayi Motaaleghi M., 2015, Aeroelastic analysis and active flutter suppression of an electro-rheological sandwich cylindrical panel under yawed supersonic flow, *Aerospace Science and Technology* **42**:118-127.

[16] Krivenkov K., Ulrich S., Bruns R., 2012, Extending the operation range of electrorhe-ological actuators for vibration control through novel designs, *Journal of Intelligent Material Systems and Structures* **23**(12): 1323-1330.

[17] Lu J.Z., Li Q.B., 2010, Application of electrorheological fluid to vibration control of structures, *Journal of Yantai University (Natural Science and Engineering)* **23**(3): 223-228.

[18] Natarajan S., Haboussi M., Manickam G., 2014, Application of higher-order structural theory to bending and free vibration analysis of sandwich plates with CNT reinforced composite, *Composite Structures* **113**: 197-207.

[19] Norrick N., 2014, Electrorheological fluid power dissipation and requirements for an adaptive tunable vibration absorber, *International Journal of Innovations in Materials Science and Engineering* **1**(2): 49-57.

[20] Pawlus D., 2016, Dynamic response control of three-layered annular plate due to various parameters of electrorheological core, *The Journal of Committee on Machine Building of Polish Academy of Sciences* **63**(1): 73-91.

[21] Poortabib A., Maghsoudi M., 2014, The analytical solution for buckling of curved sandwich beams with a transversely flexible core subjected to uniform load, *Structural Engineering and Mechanics* **52**(2): 323-349.

[22] Rafiee M., He X.Q., Liew K.M., 2014, Non-linear dynamic stability of piezoelectric functionally graded carbon nanotube-reinforced composite plates with initial geometric imperfection, *International Journal of Non-Linear Mechanics* **59**: 37-51.

[23] Rakrak K., Zidour M., Heireche H., Anis Bousahla A., Chemi A., 2016, Free vibration analysis of chiral double-walled carbon nanotube using non-local elasticity theory, *Advances in Nano Research* **4**(1): 31-44.

[24] Ramkumar K., Ganesan N., 2009, Vibration and damping of composite sandwich box column with viscoelastic/electrorheological fluid core and performance comparison, *Materials and Design* **30**: 2981-2994.

[25] Rezaeepazhand J., Pahlavan L., 2008, Transient response of sandwich beams with electrorheological core, *Journal of Intelligent Material Systems and Structures* **20**(2): 171-179.

[26] Shen H.S., Zhang C.L., 2012, Non-linear analysis of functionally graded fiber reinforced composite laminated plates, Part I: Theory and solutions, *International Journal of Non-Linear Mechanics* **47**: 1045-1054.

[27] Sun C., Li F., Cheng H., Lu G., 2005, Axial Young's modulus prediction of singlewalled carbon nanotube arrays with diameters from nanometer to meter scales, *Applied Physics Letters* **87**: 193-101.

[28] Sun Y., Thomas M., 2011, Control of torsional rotor vibrations using an electrorheological fluid dynamic absorber, *Journal of Vibration and Control* **17**(8): 1253-1264.

[29] Tabassian R., Rezaeepazhand J., 2013, Dynamic stability of smart sandwich beams with electro-rheological core resting on elastic foundation, *Journal of Sandwich Structures and Materials* **15**(1): 25-44.

[30] Tang S.J., Lumsdaine A., 2008, Analysis of constrained damping layers, including normal-strain effects, *AIAA Journal* **46**(12): 2998-3011.

[31] Thai H.T., Nguyen T.K., Vo T.P., Lee J., 2014, Analysis of functionally graded sandwich plates using a new first-order shear deformation theory, *European Journal of Mechanics A/Solids* **45**: 211-225.

[32] Tounsi A., Benguediab S., Adda Bedia A., Semmah A., Zidour M., 2013, Nonlocal effects on thermal buckling

properties of double-walled carbon nanotubes, *Advances in Nano Research* **1**(1): 1-11.

[33] Wei K., Meng G., Zhang W., Zhou S., 2007, Vibration characteristics of rotating sandwich beams filled with electrorheological fluids, *Journal of Intelligent Material Systems and Structures* **18**: 1165-1173.

[34] Weiss K.D., Coulter J.P., Carlson J.D., 1993, Material aspects of electrorheological system, *Journal of Intelligent Material Systems and Structures* **4**(1): 13-34.

[35] Yalcintas M., Coulter J.P., 1995, Electrorheological material based adaptive beams subjected to various boundary conditions, *Journal of Intelligent Material Systems and Structures* **6**(5): 700-717.

[36] Yeh J.Y., Chen L.W., 2004, Vibration of a sandwich plate with a constrained layer and electrorheological fluid core, *Composite Structures* **65**: 251-258.

[37] Yeh J.Y., Chen L.W., Wang C.C., 2004, Dynamic stability of a sandwich beam with a constrained layer and electrorheological fluid core, *Composite Structures* **64**: 47-54.

[38] Ying Z. G., Ni Y.Q., Duan Y.F., 2017, Stochastic vibration suppression analysis of an optimal bounded controlled sandwich beam with MR visco-elastomer core, *Smart Structures and Systems* **19**(1): 21-31.